Geochemical behaviour and transport of technology critical metals (TCMs) by the Tinto River (SW Spain) to the Atlantic Ocean

Carlos Ruiz Cánovas[1]*, María Dolores Basallote[1], Francisco Macías[1], Manuel Olías[1], Rafael Pérez-López[1], Carlos Ayora[2], José Miguel Nieto[1]

* Corresponding author: carlos.ruiz@dgeo.uhu.es

1. Department of Earth Sciences and Research Center on Natural Resources, Health and the Environment, University of Huelva, Campus 'El Carmen', Fuerzas Armadas s/n, 21071 Huelva, Spain.

2. Institute of Environmental Assessment and Water Research, CSIC, Jordi Girona 18, 08034 Barcelona, Spain.

Abstract

This paper addresses the behaviour of several technology critical metals (TCMs), i.e., Rare Earth Elements (REE), Y, Sc, Ga and Tl, in the Tinto River (SW Spain), quantifying their fluxes to the Atlantic Ocean, and unravelling the governing geochemical processes controlling their solubility. To accomplish this issue, a high-resolution (2-24 h) sampling was performed during the hydrological year 2017/18. Mean dissolved concentrations of 380 µg/L of REE, 99 µg/L of Y, 15 µg/L of Sc, 9.2 µg/L of Ga and 4.8 µg/L of Tl were found. Most TCMs followed a similar behaviour as sulphate and base metals through the year, exhibiting a quasi-conservative behaviour due to acidic conditions. However, dissolved Tl concentrations seem to be strongly controlled by Tl incorporation onto secondary minerals and diatoms deposited on the riverbed, especially during the dry season. The remobilization of riverbed sediments led to the transport of significant

amounts of TCMs associated with particulate matter, especially to Al- oxy-hydroxy-sulphates or Al-silicates rather than Fe precipitates (except Tl and Ga). Around 5.8 tonnes of REE, 1.3 tonnes of Y, 248 kg of Sc, 139 kg of Ga and 138 kg of Tl were annually delivered in its dissolved form by the Tinto River to the Atlantic Ocean, which constitutes around 0.09% of the dissolved global flux into the oceans of Y, 0.02% of REE, 0.01% of Ga and 0.001% of Sc.

Keywords; rare earth elements (REE); thallium, gallium, acid mine drainage (AMD); global metal fluxes.

1. Introduction

Trace elements are mainly transferred from the lithosphere to the hydrosphere by rock weathering, atmospheric deposition and by anthropogenic activities (Gaillardet et al., 2003). Lithology is a critical component controlling these processes, which in turn depends on the proportion of certain minerals in rocks and the susceptibility of each mineral to weathering (Meybeck, 2003). Rivers receiving these elements are the main sources of dissolved and particulate metals to the oceans, and consequently the predominant contributors to the geochemical composition of both ocean water and marine sediments (Carey et al., 2002). However, weathering rates and metal transport by rivers may be imbalanced by anthropogenic activities such as mining, which may boost metal fluxes. For instance, Mayes et al. (2010) quantified a minimum of 551 tonnes of Fe, 193 tonnes of Zn, 72 tonnes of Mn,19 tonnes of Pb and Cu, and lesser amounts of As and Cd annually delivered from metal mines to water bodies in England and Wales. On the other hand, Raymond and Oh (2009) claimed that S released through pyrite oxidation in coal mining could account for 28-40% of the global riverine sulphate flux.

Remarkable examples of riverine metal transport worldwide are the Tinto and Odiel rivers, located in the Iberian Pyrite Belt (IPB), one of the largest concentration of

sulphides worldwide that has been intensively mined, which are deeply polluted by acid mine drainage (AMD) processes. The annual dissolved contaminant load delivered by both rivers is huge; around 35000 tonnes of sulphate, 1700 tonnes of Fe, 650 tonnes of Zn, 410 tonnes of Cu and lesser amounts of other ions (Nieto et al., 2013). The contaminants load is important if global fluxes are considered; the load transported by both rivers represents around 0.8% and 2.8% of the global gross flux of Cu and Zn, respectively (Nieto et al., 2013). Ion transport patterns in such systems are relatively well-known for sulphate and base metal/loids, being strongly controlled by several geochemical processes (e.g. washout of soluble salts, mineral precipitation, sorption/desorption processes, or dilution by runoff). Thus, dissolved concentrations of sulphate and metals drastically increase after the first rainfalls of the rainy season due to the washout of soluble salts and sulphide oxidation products, previously stored in mine areas and riverbanks during the dry period. Then, a general decrease is observed when these soluble evaporitic salt minerals and concentrated pore waters are depleted and dilution by freshwater became the predominant process controlling dissolved concentrations. Afterwards, variations in dissolved concentrations are associated with different factors such as oxy-hydroxy-sulphate precipitation and relative changes in AMD inputs and contribution of freshwaters during the rainy events (Cánovas et al., 2008).

However, little is known about the behaviour and transport patterns in the hydrosphere of other metals such as the technology critical metals (TCMs), which include among others rare earth elements (REE), Y, Sc, Ga and Tl. These elements are of great importance in the development of emerging key technologies, electronics or the aerospace industry, and their extensive extraction has led to increasing concentrations in the hydro- and biosphere (Cobelo-Garcia et al., 2015). There is a growing interest in the last years about the transport of TCMs from rivers to oceans (e.g., Resongles et al., 2015; Lozano et al., 2020), however studies dealing with the quantification of these fluxes are scarce (e.g., Gaillardet et al., 2003; Meybeck, 2003), especially in AMD-affected

78 catchments. TCMs can be naturally found in minerals as major or minor components.
79 For instance, Ga can be incorporated into feldspars (Deer et al., 2001), while Tl can be
80 found not only in alkali micas and feldspars replacing K, Rb or Sr, but also in sulphides
81 (e.g. Law and Turner, 2011). In the case of REE, Y and Sc in AMD waters, the origin of
82 these elements is not totally clear, however previous studies suggest that these elements
83 are preferentially concentrated in host rock minerals instead of in sulphides (e.g.
84 Migaszewski et al., 2014; Cánovas et al., 2020). Although these elements are commonly
85 found at low concentrations in natural waters (Noack et al., 2014), the high acidity
86 generated in AMD may increase their concentrations up to several orders of magnitude
87 (e.g. Ayora et al., 2016; Cánovas et al., 2020).

88 Therefore, the main objectives of this study are: i) to study the behaviour of different
89 TCMs (i.e. REE, Y, Sc, Ga and Tl) in the world-famous Tinto River during one
90 hydrological year, ii) to quantify their fluxes from the mines to the Atlantic Ocean, and iii)
91 to unravel the geochemical processes that control the fluxes of these TCMs. The results
92 obtained in this study could help to fill the gap in knowledge about the behaviour and
93 transport of TCMs in environments affected by anthropogenic activities worldwide.

94 ## 2. Methodology

95 ### 2.1. Site description

96 The Tinto River mainly drains materials belonging to the IPB, which comprises three
97 different lithological groups from the Upper Palaeozoic: (i) the Phyllite-Quartzite Group
98 (PQ), composed of a sequence of phyllites and quartzites, (ii) the Volcano-Sedimentary
99 Complex (VSC), formed by a mafic-felsic volcanic sequence interstratified with shales,
100 and (iii) the Culm Group, which overlies the VSC, and is composed of shales, sandstones
101 and conglomerates. Sulphide orebodies are found in the VSC and contain primarily pyrite
102 (FeS_2) and minor quantities of chalcopyrite ($CuFeS_2$), arsenopyrite (FeAsS), sphalerite
103 (ZnS), and galena (PbS). As long as the river travels downstream, Neogene materials
104 outcrop, mainly marls and calcarenites. A complete geological information of the area

105 can be found in Tornos (2006). The mineral richness found in the Riotinto mines, as well
106 as other areas of the IPB, has led to intense and discontinuous historical mining activities
107 (e.g. Tartessians, Romans). However, the most intense mining period took place after
108 the creation of the Rio Tinto Company in 1873, when industrial- high-scale mining was
109 performed until 2001 when the mine closed due to the Cu price falls. During this period,
110 more than 140 Mt of minerals were extracted in the Riotinto mines, leading to a drastic
111 increase in metal pollution levels in the Tinto river catchment (Olías and Nieto, 2015). At
112 the Peña de Hierro mining complex (Fig. 1), the Tinto River is originated by the
113 confluence of several drainages flowing out of different wastes piles.

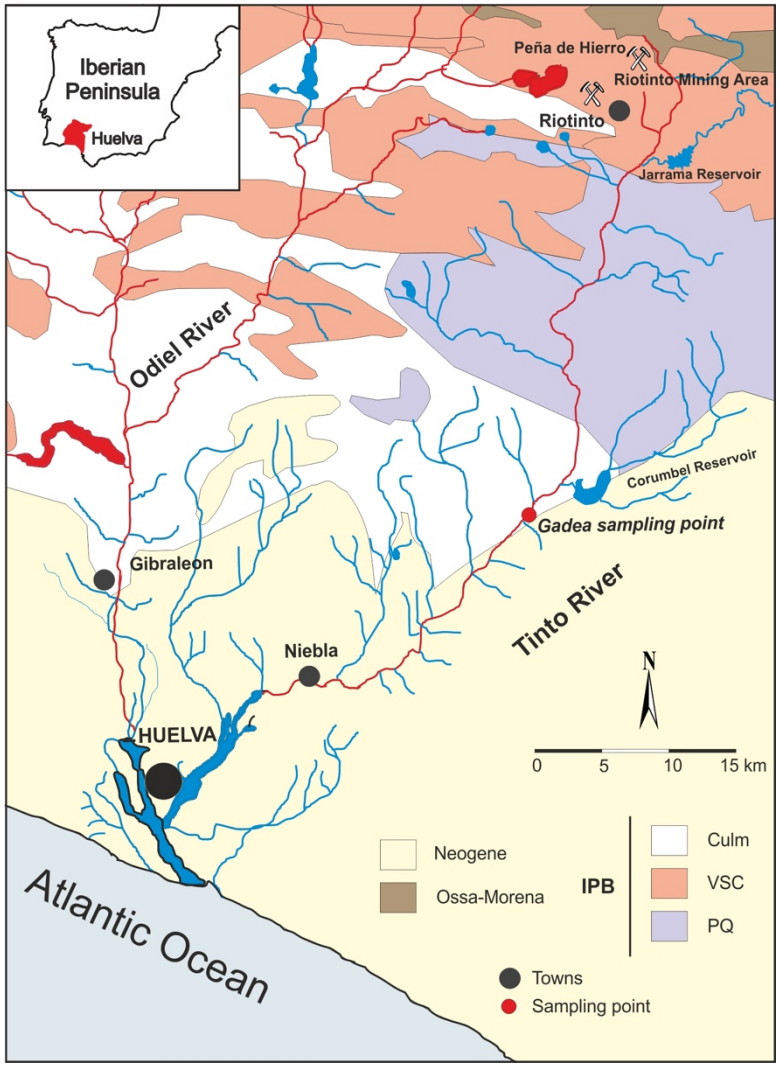

114

115 **Figure 1.** Geological map of the Tinto River basin, including the location of mine sites
116 and sampling point. Water affected by AMD are represented in red colour.

117 Some kilometres downstream, the Tinto River is fed by countless acidic discharges from
118 underground galleries, spoil heaps, settling ponds, and tailing dams located in the
119 Riotinto mining complex. Downstream of this vast mining area, the river does not receive
120 any other AMD input and its main tributaries (i.e. Jarrama Creek and Corumbel River;
121 Fig. 1) are regulated by pristine water reservoirs (capacity of 43 and 19 hm^3,
122 respectively).

123 The climate is of a dry Mediterranean type with an average rainfall ranging from 500 mm
124 in the lower part of the catchment to 800 mm in the northern part, although a high
125 variability is observed through the year. However, around 70% of the annual rainfall is
126 recorded from October to February, while scarce rainfalls are usually collected during
127 the dry period (from June to September) (Olías et al., 2006). The Tinto basin is composed
128 mainly of impermeable materials; therefore, the river has a low natural regulation, and
129 most of the water discharge occurs during flood events. The average river contribution
130 is around 7.2 m^3/s, although with a high variability, strongly linked to the rainfall regime
131 (Olías et al., 2006). Together with the Odiel, another acid river, the Tinto River discharges
132 into the Atlantic Ocean through the Huelva estuary.

133 ## 2.2. Sampling and analysis

134 A high-resolution sampling was performed in the Tinto River during the hydrological year
135 2017/18 at the Gadea station (Fig. 1), which is around 20 km upstream the estuary. The
136 sampling was scheduled depending on the weather forecast; sampling frequency ranged
137 from 2 to 24h. A total of 590 samples were collected, however, only those samples
138 showing variations (> 20%) in electrical conductivity (EC) values were selected for
139 analysis (n=143). The number of selected samples for analysis varied sharply during the
140 study period according to rainfall-induced hydrochemical variations, with 65 samples
141 collected in March 2018 and only 2 samples selected in summer.

142 Sampling was performed using a Teledyne ISCO autosampler equipped with a 24-bottles
143 container, washed with dilute acid (10% v/v HNO_3) before each sampling cycle.
144 Scheduled purge sequences were made in order to avoid cross-contamination between
145 pumping cycles. Manual samples were collected coinciding with the beginning of each
146 autosampler sequence for comparison purposes. Different physico-chemical parameters
147 such as pH, EC, oxidation-reduction potential (ORP) and temperature (T^a) were
148 measured in each sample using a Crison MM40+ equipment previously calibrated. The
149 ORP readings in the field were converted to redox potential values referred to the
150 standard hydrogen electrode (Eh) (Nordstrom and Wilde, 1998). Samples were filtered
151 through 0.45 µm Millipore Teflon filters and acidified with ultrapure HNO_3 Merck to pH <
152 1 and stored refrigerated until analysis. Unfiltered aliquots (n=53) were taken from
153 samples collected during floods and acidified to determine the metal particulate transport
154 following the procedure of Garbarino and Hoffmann (1999); the difference in
155 concentration between the filtered and unfiltered samples is considered as associated to
156 particulate matter.

157 Rainfall data were obtained from two gauge stations located at the north and south of
158 the river basin (Fig. 1). Flow information was obtained at quarter-hourly intervals from
159 the Gadea streamflow gauge station (Fig. 1), which belongs to the gauging streamflow
160 network of the Andalusian Water Agency. Data of water releases from the Corumbel and
161 Jarrama reservoirs were also obtained.

162 Samples were analysed by Inductively Coupled Plasma-Atomic Emission Spectroscopy
163 (ICP-AES; Perkin-Elmer® Optima 3200 RL) for major elements and by Inductively
164 Coupled Plasma-Mass Spectroscopy (ICP-MS; Perkin-Elmer®SciexElan 6000) for trace
165 elements. Detection limits were 200 µg/L for Al, Ca, Fe, K, Mn, Mg, Na and S; 50 µg/L
166 for Zn; 5 µg/L for Cu; and 0.1 µg/L for As, Co, Cr, Ga, Ni, Pb, Sc, Tl, and Y. The detection
167 limits for REEs ranged from 0.5 µg/L for La, Ce, Nd, Pr and Sm to 0.2 µg/L for Eu, Gd,
168 Tb, Dy, Ho, Er, Tm, Yb and Lu. The sulphate concentration was calculated from the

169 stoichiometric relationship (1:3) between sulphate and S in samples, considering that S
170 is entirely found as sulphate. This estimation was checked from the speciation obtained
171 by the geochemical code PHREEQC (Parkhurst and Appelo, 2013). The accuracy of the
172 analyses was corroborated with a NIST-1640 (NIST, USA) certified reference material
173 and by laboratory control materials prepared from certified materials and used during
174 each analysis sequence. The agreement between the determined and certified and/or
175 reference values was better than ± 6% for all elements studied. The analytical precision
176 was assessed performing triplicate analyses, being better than 5% for all cases. The
177 average balance error obtained by the PHREEQC code v3.4 (Parkhurst and Appelo,
178 2013) was 2.4% (interquartile range between -0.4 and 4.8%).

179 ## 2.3. Pollutant load estimation and saturation indices

180 Pollutant loads delivered by the Tinto River were calculated from element concentrations
181 and flow measurements by interpolating concentrations between two consecutives
182 samples according the following equation:

183 $$C_i = \frac{C_n - C_{n-1}}{t_{n-}t_{n-1}}(t_i - t_{n-1}) + C_{n-1}$$

184 Being C_i the concentration at the time i, C_{n-1} and C_n the concentrations of the available
185 samples before and after the time i ant t_n and t_{n-1} the dates of samples C_n and C_{n-1}. Thus,
186 the concentrations were obtained every 15 minutes and multiplied by the corresponding
187 river flow for obtaining the instantaneous pollutant loads. Finally, monthly loads were
188 calculated from instantaneous loads. This may be considered as an approach since the
189 gauge station is located 20 km upstream the estuary and the interaction of calcarenites
190 and marls with the Tinto waters in this river section may cause the precipitation of Fe
191 and other trace metal/loids (i.e., As, Pb, or Cu; Cánovas et al. 2014).

192 Saturation indices (SI) of water were obtained using the PHREEQC code v3.4 (Parkhurst
193 and Appelo, 2013) using the Minteq.v4 thermodynamic database (Allison et al., 1999).

194 The database was amended with equilibrium constants (Ke) of schwertmannite from
195 Sánchez-España et al. (2011).

196 ## 3. Results and Discussion

197 ### 3.1 Rainfall distribution and discharge evolution

198 The rainfall collected during the hydrological year 2017/18 was quite similar to mean
199 annual values (i.e. from around 500 to 800 mm in the southern and northern parts of the
200 basin, respectively), with a marked uneven distribution of rainfalls. The rainfall collected
201 from July 2017 to February 2018 only accounted for 163 mm. In contrast, intense rainfall
202 episodes between March and April 2018 generated a total precipitation of around 457
203 mm, that is, almost 67% of the annual rainfalls (Fig. 2A). This rainfall trend contrasts with
204 the common rainfall distribution observed in this area, with most rainfall concentrated
205 from October to February (Olías et al., 2006).

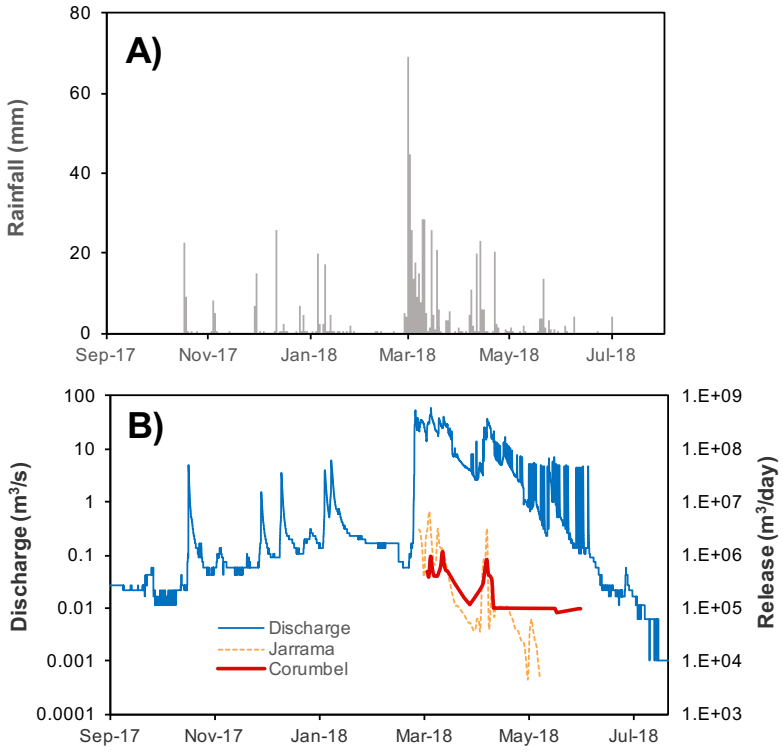

206

207 **Figure 2.** A) Rainfall collected during the study period and B) evolution of the Tinto river
208 flow, including the contribution from freshwater reservoirs (Corumbel and Jarrama).

Due to the low permeability of the basin materials, this rainfall distribution had a strong influence on the river flow evolution during the study period. The river flow remained below 0.025 m^3/s before October 2017, however the first rainfalls recorded after summer (on October 17th and 18th) led to a sharp increase up to a maximum value of 4.7 m^3/s on October 18th (Fig. 2B). Similar rainfall episodes were observed until February, leading to some discharge peaks, though lower than 6 m^3/s. At the end of February, the river flow remained close to 0.13 m^3/s owing to the absence of rainfalls. However, an intense rainfall period recorded afterwards caused a sharp flow increase, reaching a value of up to 52 m^3/s on March 1st. These high-flow conditions (above 10 m^3/s) persisted until mid-April partly due to the releases from water reservoirs located in the basin (Fig. 2B). Then, the river flow progressively decreased down to 0.001 m^3/s in summer, however a daily zig-zag evolution of river flow during May and June was observed, probably as a consequence of water releases from reservoirs, however it cannot be ruled out the influence of pumped water from the Riotinto mine. Unfortunately, no data from these discharges are available (Fig. 2B).

3.2. Evolution of dissolved concentrations of AMD-related elements

The evolution of some dissolved element concentrations for the whole period is shown in Figure 3, however, detailed evolution of elements during flood episodes can be seen in Figure SM1. The first rainfalls recorded in October gave rise to increasing dissolved concentrations of sulphate (from 2466 to 12156 mg/L) and metals (e.g. Fe, from 162 to 1529 mg/L) (Fig. 3), barely 4 days after the beginning of rainfalls, due to the dissolution of sulphate efflorescent salts precipitated during the summer on the riverbanks and mine sites. These concentrations constituted the highest concentrations during the study period (Table SM1). The EC values also followed the same evolution (not shown in Fig. 3). The acidity stored in efflorescent salts led to the decrease of pH values (from 2.44 to 2.15; Fig. 3) after their dissolution. These washout processes have been previously reported both in the IPB and other mine sites worldwide (e.g. Jamieson et al., 2005;

Cánovas et al., 2008). Afterwards, a progressive decrease in dissolved concentrations was observed although values were still high (e.g., EC values from 11.4 to 3.5 mS/cm, from 12156 to 1323 mg/L of sulphate and from 1529 to 149 mg/L of Fe; Fig. 3). This high level of dissolved pollutants in the river was enhanced by the lack of dilution processes induced by rainfalls and the continuous transport of sulphide oxidation products from the mine site to the river, although the latter lost progressively importance in winter.

The intense rainfall events observed in March and April gave rise to a sharp increase in pH values (mainly above 3, with a maximum of 4.2; Fig. 3) and a decrease in EC, and dissolved concentration of sulphate and metals (e.g. down to 0.38 mS/cm, 112 and 0.05 mg/L of sulphate and Fe, respectively; Table SM1) although with sharp variations in response to changes in river flow. In this sense, an initial increase in concentrations was observed (Fig. 3) due to washout of soluble sulphate salts accumulated between rainfall events. It is also noteworthy that while the highest discharges were recorded at the beginning of March, the highest pH values and the lowest concentrations were reached in mid-April due probably to the progressive exhaustion of sulphide oxidation products from the mining area. From mid-April onwards, EC, pH and dissolved concentration values started to recover coinciding with decreasing river flows (Fig. 3).

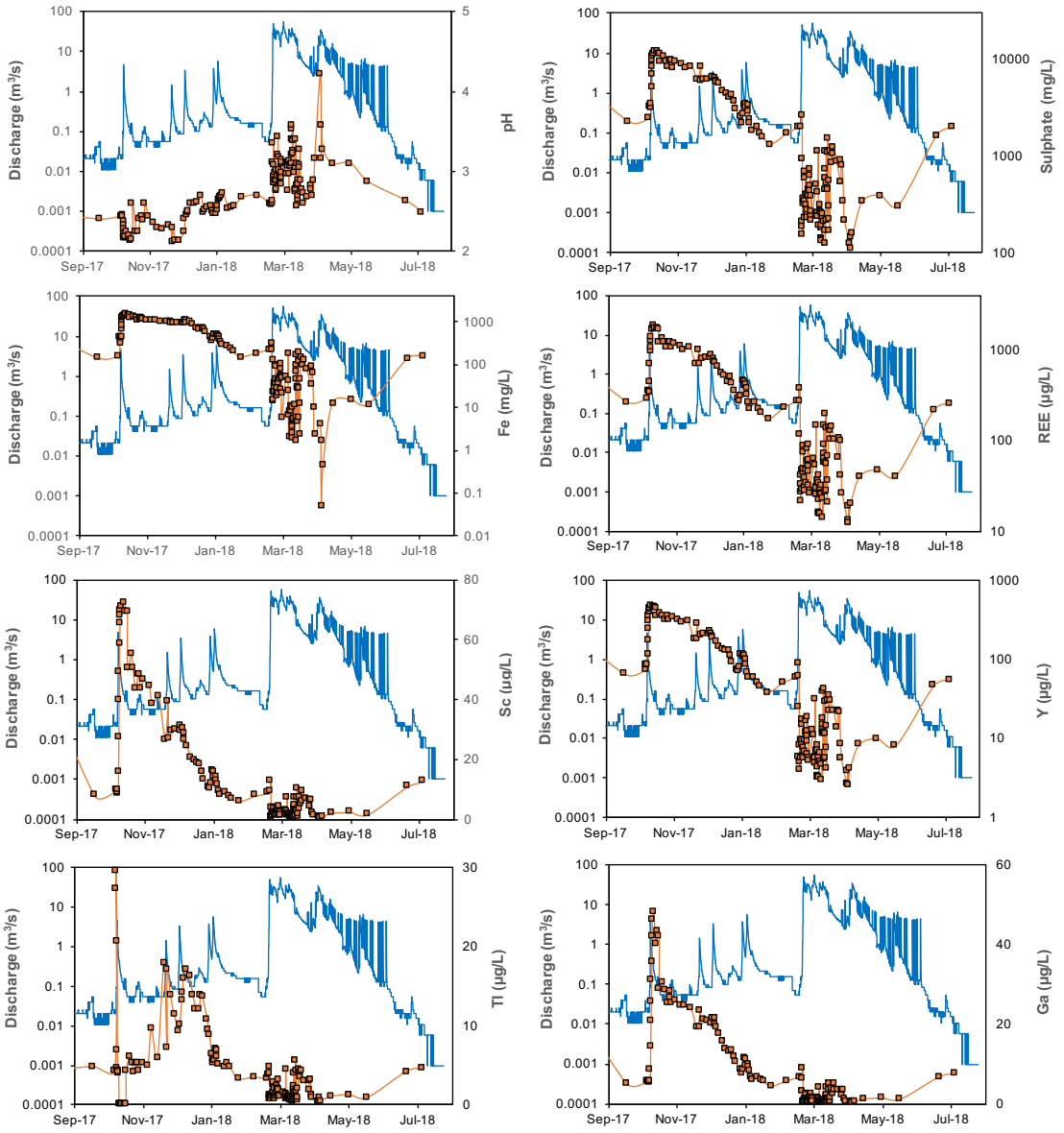

253

254 **Figure 3.** Evolution of pH and dissolved concentration of sulphate, Fe and selected
255 TCMs in the Tinto River during the study period.

256 **3.3. Evolution of TCMs dissolved concentrations**

257 Some basic statistics of dissolved concentrations of TCMs can be seen in Table SM2. A
258 similar evolution than that observed for sulphate (and base metals) was recorded, except
259 for Tl (Fig. 3). After the first rainfalls recorded after summer, the dissolved concentration
260 of TCMs increased notably in the river, although with some differences among metals.
261 The highest increase in concentration was observed for Ga (> 8 times, from 5.6 to 49
262 µg/L), followed by Sc (7 times, from 10 to 72 µg/L) and REE and Y, which increased

more than 6 times their concentrations in the river (from 298 to 1856 µg/L, and 74 to 478 µg/L, respectively; Fig. 3).

In the case of Tl, the concentration peak did not coincide with the maximum values for the rest of metals (4 days after the rainfalls beginning), but a few hours after the onset of rainfalls (up to 29 µg/L; Fig. 3). In fact, it is noteworthy that Tl concentrations were below the detection limit coinciding with the highest concentrations for the rest of TCMs (also for base metals). The increases observed for TCMs (6-8 times > pre-rainfall values) associated to washout processes were higher than those recorded for sulphate and Fe (around 3.5 times), main components of evaporitic sulphate salts assemblage precipitated during summer in AMD environments (Jamieson et al., 2005).

Other major components of evaporitic sulphate salts such as Al, Mg and Ca (e.g. alunogen, hexahydrite and gypsum, respectively) found in minor quantities in AMD environments (Jamieson et al., 2005) also underwent a lower increase than TCMs (2 times for Ca, 4 times for Mg, and 5 times for Al) after rainfalls. However, if compared with increases observed for trace metals such as Cu, Zn, Co, Ni or Cd, commonly included in the mineral structure of evaporitic sulphate salts as impurities, similar increases than those for TCMs were observed (between 6-7 times). That is, the washout processes of evaporitic salts in AMD environments may induce a greater enrichment in most trace metals in the river waters than major component of evaporitic salts.

After these washout processes, the concentration of most TCEs decreased progressively until the rainfall episodes of March; from 1856 to 172 µg/L of REE, from 478 to 38 µg/L of Y, from 72 to 6.0 µg/L of Sc, and from 49 to 4.4 µg/L of Ga (Fig. 3). Once again, Tl deviates from the general trend observed for the rest of TCMs, with increasing concentrations associated to the rise in river flow observed in November and December, reaching up to 18 µg/L; Fig. 3). Afterwards, with the rainfall events of January, Tl concentrations decreased progressively until reaching values (3.3 µg/L of Tl) even lower than those recorded at the beginning of the study period. As in the case of sulphate

290 (and base metals), the concentration of TCMs initially increased during the intense
291 rainfalls of March, but immediately decreased due to dilution by runoff, exhibiting
292 fluctuations induced by the different flood events recorded. During these events, the
293 lowest concentrations of the year were observed; 13 µg/L of REE, 2.5 µg/L of Y, 0.43
294 µg/L of Sc, 0.33 µg/L of Tl and 0.10 µg/L of Ga. Finally, the concentration of TCMs
295 increased progressively until summer coinciding with the absence of rainfalls (Fig. 3).

296 As can be seen in Figure 4, REE, Y, Sc and Ga followed a similar evolution to sulphate
297 for the whole period. Thus, correlation coefficient (R^2) values above 0.98 were found
298 among sulphate and REE, Y, Sc and Ga. However, a different evolution is observed for
299 Tl, which does not correlate with the rest of TCMs and sulphate (e.g., R^2 = 0.13 for Sc
300 and R^2 = 0.20 for Ga; Fig. 4). Comparing the evolution of Tl with the rest of TCMs
301 (represented by Ga) during the short flood events from two different periods, i.e. from
302 September to February and from March on (Fig. 5), it can be observed that there is no
303 correlation between both TCMs during the first period (Fig. 5A and B). However, the
304 intense rainfall events recorded mainly in March and April, with discharge values above
305 50 m^3/s, caused a similar response for all TCMs including Tl, displaying strong
306 fluctuations associated to river flow (Fig. 5C). At this point, the storage of evaporitic
307 sulphate salts in mine sites is completely exhausted and TCMs concentration may be
308 controlled by the relative contribution of runoff from the catchment and AMD from the
309 mining area. Thus, unlike the dry period, where no correlation was observed between Tl
310 and the rest of TCMs, a high correlation (R^2 = 0.93) was recorded during the rainy period
311 (Fig. 5D).

312

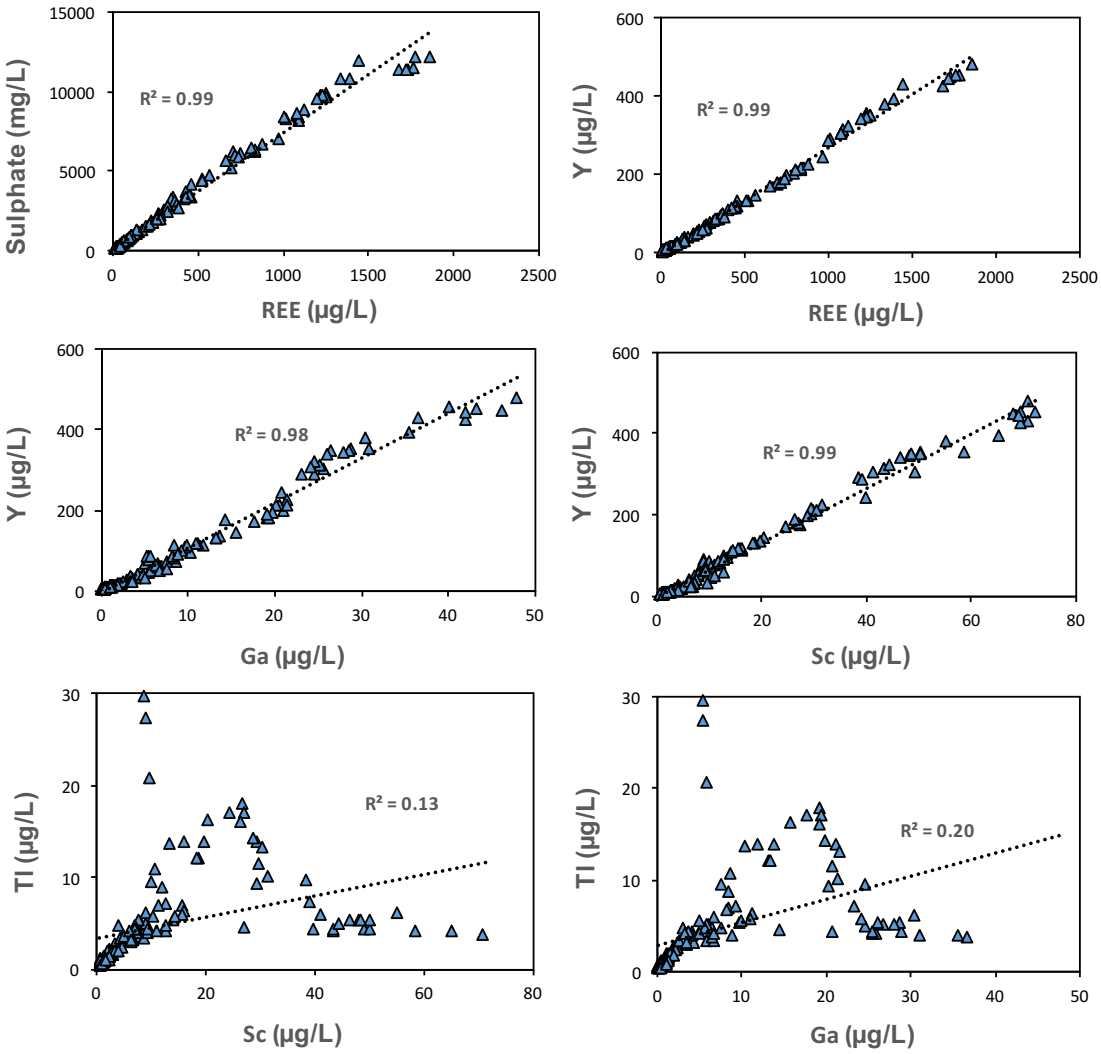

313

314 **Figure 4.** Relationships between the dissolved concentration of some TCMs studied in

315 the Tinto River.

316

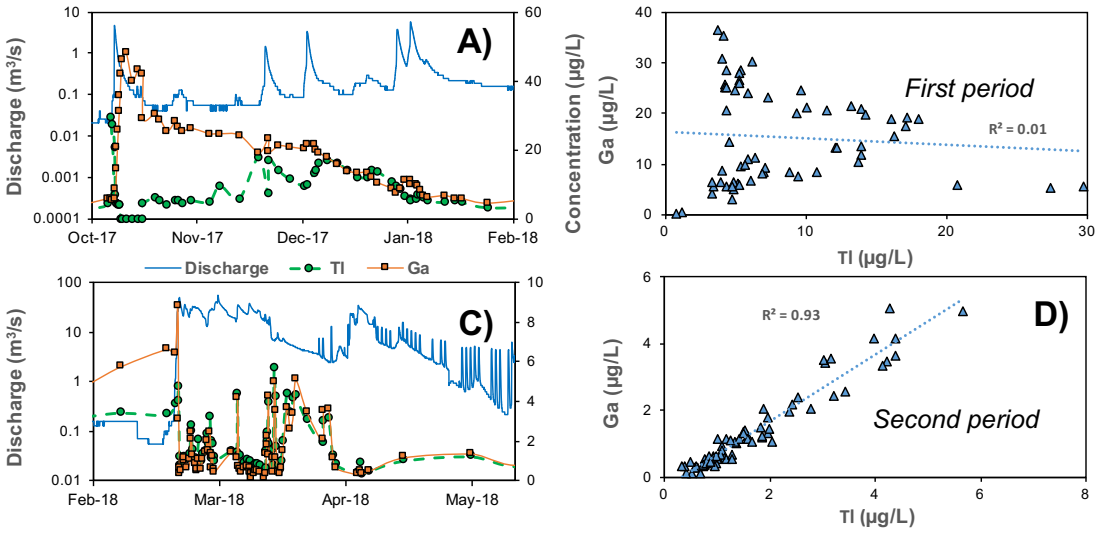

317

318 **Figure 5.** Comparison of the dissolved concentration of Ga and Tl during different
319 periods (First; from October to February, Second; from March to May) associated to
320 rainfall intensity.

321 **3.4. Particulate concentrations of TCMs during floods**

322 Metal transport in AMD chiefly takes place by the dissolved phase owing to the low pH
323 values found. However, flood events may alter this metal transport pattern by both
324 mineral precipitation after sharp pH increases and metal-rich loose sediment
325 remobilization, leading to high particulate metal concentrations (e.g. Cánovas et al.,
326 2012; Resongles et al., 2015). In the case of the TCMs studied, an average particulate
327 concentration of 5.7 µg/L of REE was observed, although with maximum values of 78
328 µg/L (Table SM2). Lower average particulate concentrations were observed for Y (1.3
329 µg/L, with maximum of 21 µg/L), Ga (0.59 µg/L, and 6.1 µg/L), Sc, (0.36 µg/L, and 4.0
330 µg/L) and Tl (0.32 µg/L, and 4.0 µg/L; Table 2). Although a high variability is observed,
331 around 29% (mean value) of Ga, 14% of Sc, 12% of Tl and around 9% of REE and Y in
332 the water would correspond to particulate matter (Figure SM2). These values (except for
333 Ga) are similar or slightly higher than those observed for other lithophile metals such as
334 Si (7.7%) or Al (4.4%), but noticeably lower than those observed for other elements
335 associated to sulphides such as As, Fe and Pb (71%, 40% and 20% of total, respectively;

Fig. SM2). A comparison between the content of TCMs and other metals in the particulate matter could shed light on the origin of TCMs. Thus, Figure SM3 shows the relationship among different metals in the particulate matter transported by the Tinto River during floods. The presence of REE in the particulate matter could be associated to remobilized aluminosilicate rather than Fe precipitates, as evidenced by the linear relationship between particulate REE and Al and Si (R^2 = 0.74 and 0.52, respectively; the latter not shown in Fig. SM3), which is not observed for Fe. Scandium (R^2 = 0.94) and to a lesser extent Y (R^2 = 0.79) also showed a linear relationship with REE, pointing at a similar source within the particulate matter. However, other mineral phases could carry REE, Y and Sc in AMD environments. For example, an oxy-hydroxy-sulphate known as basaluminite ($Al_4SO_4OH10{\cdot}5H_2O$) has been reported as a good scavenger of REE and Sc in AMD environments (Lozano et al., 2020). The high correlation between these metals (i.e. REE, Y and Sc) and sulphur (R^2 = 0.81-0.83) in the particulate matter (Fig. SM3) would support this possibility. Although this mineral tends to precipitate at pH values higher than 4, which were only temporally achieved in the river (max. 4.2; Table SM1), this precipitation may have occurred in the confluence of the Tinto river with freshwater tributaries, and the mineral particles of basaluminite subsequently transported by the particulate matter until the sampling point. However, this hypothesis must be further tested.

On the other hand, Ga usually exhibits a similar geochemical behaviour to Al (Shiller and Frilot 1996), therefore it could be hosted by aluminosilicates remobilized during the floods. However, while a high correlation is observed with Si (R^2 = 0.78) and Fe (R^2 = 0.85), a poorer value was recorded with Al (R^2 = 0.13). In this sense, Ga can be incorporated in jarositic minerals as impurity, replacing Fe(III) in the mineral structure (Dutrizac and Chen, 2000). These precipitates commonly coat clay minerals deposited in the riverbed sediments. As in the case of Ga, Tl was also associated with both Si (R^2 = 0.87; Fig. SM2) and Fe (R^2 = 0.67; Fig. SM3). Jarosite is considered as a strong

363 scavenger of Tl by both K and Fe(III) substitution (Dutrizac et al., 2005). The precipitation
364 of this mineral has been widely reported in the IPB (e.g. Sánchez-España et al., 2005)
365 and particularly in the Tinto River (e.g. Cánovas et al., 2008; López-Arce et al., 2019).
366 However, no linear correlation between particulate K and Tl was observed in collected
367 samples (not shown in Fig. SM2). This fact could be attributed to a preferential
368 substitution of Tl instead of K in jarosite. On the other hand, although the high affinity of
369 Tl(I) to be adsorbed on clays has been previously reported (Vögelin et el., 2015), the low
370 pH values found in the river suggest that adsorption processes on clays must be of minor
371 importance. The high correlation of Tl with Si (and not with Al) could be explained by the
372 coating of clay particles by jarosite precipitates, like in the case of Ga. However, previous
373 studies (Gómez-González et al., 2015) suggest the incorporation of Tl in the siliceous
374 frustules of diatoms. These organisms are profusely found in AMD environments,
375 particularly in the particulate matter transported by acidic rivers (Cánovas et al., 2012).

376 The particulate matter concentration in the river is strongly controlled by the river flow,
377 especially during high flood events, which cause the remobilization of riverbed
378 sediments. However, the highest particulate concentration of most base metals and
379 TCMs does not generally coincide with the highest river flow values (except in the case
380 of Pb; Fig. SM4) and depends mainly on the nature of the particulate matter (e.g.,
381 presence of Fe/Al oxyhydroxisulfates, aluminosilicates, etc.), transported by the river.

382 **3.5. Geochemical controls of TCMs solubility**

383 The precipitation of secondary minerals is an important natural attenuation mechanism
384 in AMD-affected environments (Nordstrom, 2011), which has been widely reported in the
385 Tinto River (e.g. Cánovas et al., 2008; 2010). As shown in Figures 3 and 4, most TCMs
386 exhibit the same response to sulphate, showing a sharp increase with the washout of
387 soluble salts. The mineralogy and chemical composition of these sulphate salts depend
388 strongly on the chemical composition of precipitating solutions (Buckby et al., 2003),
389 thus, if initial waters contain significant concentrations of TCMs, it is reasonable to expect

its retention in these minerals upon strong evaporation processes and its release after dissolution. However, Tl exhibits a different behaviour than other metals, peaking its concentration a few hours after the first rainfalls and remaining below the detection limit coinciding with most metal concentration peaks (Figs. 3 and 5A). It is worth to note that dissolved Tl behaviour is quite similar to that of K during the first flood (Fig. SM5). As stated before, both elements are found in jarosite minerals. Therefore, the earlier concentration peak of Tl (and K) could be attributed to proton substitution processes in the jarosite minerals as a consequence of the acidity released by the dissolution of highly-soluble evaporitic salts with the first rainfalls. However, an alternative hypothesis could be proposed related to the incorporation of Tl in diatoms. The siliceous surface of diatoms contains highly-reactive functional groups with both protons and metal ions (Gonzalez-Davila et al., 2000). Thus, once the protons released during the washout of soluble salts contact the diatoms frustules, Tl could be released to the river water and protons incorporated to the diatoms.

Once the evaporitic soluble salts are mainly re-dissolved by the first rainfalls, other secondary minerals may gain importance in instream metal sequestration. The high Fe(III) concentrations in AMD environments lead to the precipitation of a mixture of Fe minerals of uncertain composition and crystallinity such as jarosite, schwertmannite and ferrihydrite (Nordstrom, 2011). These minerals have a great sorption capacity for dissolved trace metals (e.g. Acero et al., 2006; Lozano et al., 2020), however, this process is very sensitive to the mineral structure, for instance, schwertmannite has a greater sorption capacity than ferrihydrite at a given pH (Webster et al., 1998). Figure SM6 shows the saturation indices in the Tinto waters of main Fe precipitating minerals in AMD environments. As can be seen, Tinto waters were oversaturated with respect to jarosite most of time, especially during the dry season, when isolated rainfall episodes took place.

However, saturation indices decreased noticeably from March floods on, even reaching subsaturation values, and gaining importance schwertmannite precipitation with values close to equilibrium during this period (Fig. SM6). Assuming a conservative behaviour of sulphate in AMD, i.e. the removal by oxy-hydroxy-sulphate/sulphate is negligible compared to the high dissolved concentrations (e.g. Berger et al., 2006), the incorporation of most TCMs onto these minerals seems to be of minor importance in Tinto waters at the pH range studied (2.1-4.2), as evidenced by the high correlation between dissolved sulphate and REE (Fig. 4). In this sense, Lozano et al. (2020) recently reported that REE and Y are effectively sorbed onto schwertmannite at pH values from 4.5 to 6.5, while Sc sorption occurred at a lower pH, from 3 to 5. In the Tinto waters, despite that 25% of samples exhibited pH >3 (percentile 75^{th} of 3.02; Table 1), coinciding with the rainy period when schwertmannite precipitation may be favoured, sorption may play a negligible role on REE, Y and Sc solubility.

Other TCMs such as Tl and Ga exhibited a high correlation with both Si and Fe in the particulate matter (Fig. SM3). However, both elements behave differently in the dissolved fraction; while Ga behaves like the rest of TCMs, Tl follows a singular evolution. Thallium increased its concentration coinciding with the general decrease in concentration for most TCMs after the washout of soluble salts (Fig. 3). This evolution is similar to that observed for As, whose concentrations peaked in mid-December, and is strongly adsorbed/coprecipitated onto Fe oxy-hydroxy-sulphates (Casiot et al., 2003). This process constitutes an important attenuation process in evolved mine waters downstream of mine sites. This evolution of As in the Tinto River has been recently addressed by Olías et al. (2020) to the arrival of less evolved water coming from the mining area to the sampling point. This water is less affected by Fe precipitation and therefore has higher concentrations of As and Tl. As can be seen in Figure 6, the high concentrations of Tl observed in November and December (Fig. 3) are associated with the highest Fe/SO_4 ratio, which indicate less Fe precipitation (Olías et al., 2004). On the

contrary, the lowest values of Tl are reached with the lowest Fe/SO_4 ratios due to the intense Fe precipitation. Thus, except during the quick acid-induced desorption processes from diatom frustules or jarosite with the first rainfalls, which led to the highest Tl concentrations of the year, Tl follows a similar evolution to As (Fig. 6).

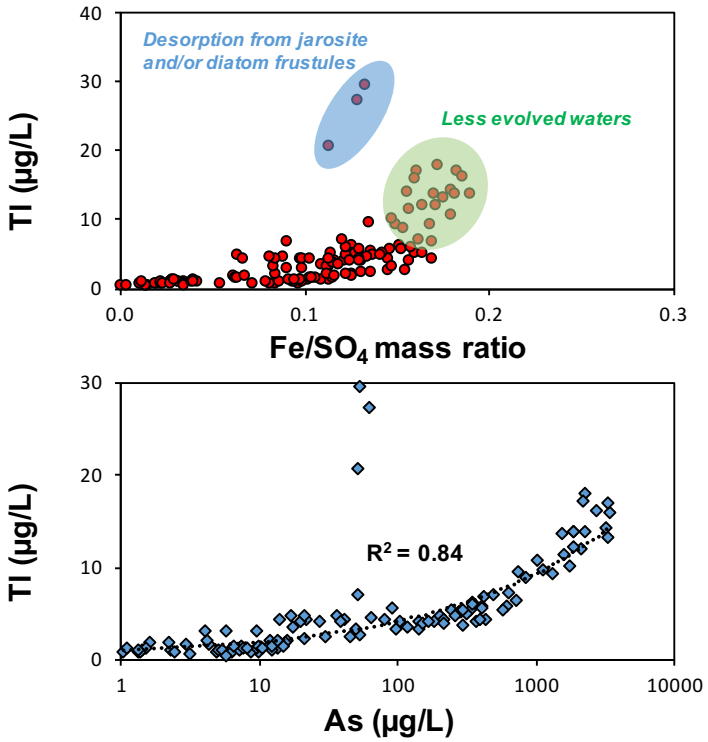

Figure 6. Relationship between the dissolved concentration of Tl and As, and the Fe/SO_4 ratio (see text for explanation).

3.6. Load of AMD-related elements and TCMs delivered by the Tinto River to the ocean

A rough estimation of metal loads delivered by the Tinto River can be made from discharge and concentration data. Around 5.8 tonnes of REE, 1.3 tonnes of Y and lesser amounts of Sc (248 kg), Ga (139 kg) and Tl (138 kg) were delivered in its dissolved form by the Tinto River (Table 1), which are different orders of magnitude lower than for other base metals. These are the first estimations performed about the transport of TCMs in

458 the Tinto River, thus a comparison with other periods is not possible. However, loads for
459 sulphate and base metals have been previously performed. The annual load of sulphate
460 (around 49000 tonnes; Table 1) transported by the Tinto River during the hydrological
461 year 2017/18 was slightly higher than average values reported by Olías et al. (2006) for
462 the period 1995/2003 (around 36600 tonnes), while Fe and Cu loads were quite similar
463 (around 5000 and 500 tonnes, respectively). It is noteworthy that the rainfall collected
464 during 2017/18 (685 mm) was lower than the average rainfall recorded for the period
465 1995/2003 (981 mm). It is also striking the lower values of As loads recorded in 2017/18
466 (around 3.6 tonnes; Table 1) compared to 1995/2003 (12 tonnes), which may be due to
467 the uneven rainfall distribution observed in 2017/18, and the extreme As values recorded
468 in 2000, coinciding with the closure of Riotinto mines (Olías et al., 2020).

	Discharge	Fe	Sulphate	Cu	As	REE	Y	Tl	Sc	Ga
	Mm^3	*ton*	*ton*	*ton*	*kg*	*kg*	*kg*	*kg*	*kg*	*kg*
Sep	0.07	22	252	2	4.0	30	8.2	0.30	1.2	0.7
Oct	0.42	314	2773	26	64	377	98	3.6	14.6	8.6
Nov	0.25	268	2058	20	203	253	71	2.1	9.8	5.9
Dec	0.71	655	4109	38	1508	518	133	8.9	18.8	13.2
Jan	1.7	702	4559	45	917	574	145	11.0	20.0	14.5
Feb	0.7	198	1621	17	98	209	47	2.6	6.9	4.9
Mar	59.2	2408	25103	307	739	2895	587	84.3	128.3	63.8
Apr	22.6	261	6424	74	44	678	140	18.5	34.5	18.7
May	4.4	77	1788	20	5.4	199.8	41.1	4.8	9.6	5.6
Jun	0.7	50.5	647	6.9	5.9	79.1	16.8	1.6	3.8	2.4
Jul	0.02	4.1	48	0.51	0.49	5.9	1.3	0.11	0.29	0.17
Aug	0.01	3.0	38	0.37	0.31	4.5	1.0	0.07	0.21	0.12
Total	91	4963	49420	556	3589	5824	1289	138	248	139
World flux[1] (ton)		2470000		55000	23000	28040	1500	-	45000	1100
Tinto contribution		0.20%		1.0%	0.02%	0.02%	0.09%		0.001%	0.01%

469 *1. Gaillardet et al. (2003)*

470 **Table 1.** Dissolved loads of sulphate, Fe, Cu, As and selected TCMs delivered by the
471 Tinto River to the Atlantic Ocean during the study period.

472 The scarcity of rainfalls from September to February led to the progressive washing of
473 evaporitic soluble salts and sulphide oxidation products, persisting this process a longer

474 time than usual. For this reason, the transport of TCMs during such period accounted for
475 20% (Tl) to 39% (Y) of TCMs of the annual loads (Fig. SM7) delivered by the Tinto River,
476 despite carrying only a 4.2% of the annual river flow. The importance of these
477 geochemical processes on the trace metal transport is highlighted by the figures
478 exhibited for As, with a 77% of the annual load, delivered during the dry season. In the
479 case of the rainy period (March-May), 95% of the annual river flow was carried by the
480 river, transporting between 60% (Y) and 78% (Tl) of TCMs annual loads. Despite the
481 negligible Tinto river flow contribution (90 Mm^3/yr; Table 1) respect to other large rivers
482 worldwide, its importance on the global dissolved trace metal fluxes to oceans is
483 evidenced if compared to fluxes reported by Gaillardet et al. (2003). Thus, the Tinto River
484 may transport into the oceans around 0.09% of the dissolved global flux of Y, 0.02% of
485 REE, 0.01% of Ga and 0.001% of Sc (Table 1). Unfortunately, no data for Tl was included
486 in Gaillardet et al. (2003). However, the contribution of Tinto River to the global fluxes of
487 TCMs is noticeably lower than that of base metals (i.e., Fe, Cu or Zn) due to its higher
488 reluctance to be remobilized by rocks than base metals in AMD environments. For
489 instance, the Cu and Fe loads transported by the Tinto River during 2017/18 would
490 constitute around 1.0% and 0.20% of the global fluxes to the oceans.

491 It is worth to mention that these dissolved loads are referred to the riverine section just
492 before the confluence with seawater. After this mixing, the pH increases drastically up to
493 pH 7 leading to the transference from the water column of most non-conservative metals
494 (e.g. Fe, Al, Pb, Tl and to a lesser extent Cu, REE and Mn) to the particulate matter,
495 which travels outside the estuary, and the sediments, leading to a metallic enrichment in
496 the estuarine sediments. On the other hand, other more conservative elements such as
497 Cd and Zn are mainly affected by dilution and travel outside the estuary to the Ocean.

498 Another important metal transport pattern, especially during intense flood episodes, is
499 that associated to particulate matter. The direct precipitation of Fe minerals when pH
500 values exceed 3, together with the remobilization of Fe precipitates from the riverbed led

to increasing particulate metal loads during floods. For example, Cánovas et al. (2012) reported in the adjacent Odiel River that the transport of total Fe (particulate+dissolved) was 37 times higher than dissolved, almost 7 times higher for Pb, and 5 times higher for Cr. Considering the values of particulate concentration of TCMs, it can be considered that the particulate transport of TCMs by the Tinto River during flood events may account for 10% to 30% of the total loads. That means that the contribution of particulate TCMs to the oceans by the Tinto River would be of minor importance and associated to intense and irregular flood events, unlike in other rivers worldwide. For example, Silva et al. (2018) reported REE fluxes of around 20 t/yr associated to suspended sediments in Ipojuca River, one of the most polluted rivers in Brazil. In this sense, rivers affected by mining activities could constitute important contributors to dissolved and particulate metals, speeding up weathering reactions of rocks.

Conclusions

This paper studies the behaviour of different TCMs in the Tinto River (SW Spain), quantifying their fluxes from the Riotinto mines to the Atlantic Ocean and unravelling the geochemical processes that control these fluxes. TCMs concentrations several order of magnitude higher than those found in natural waters were found in this study. Most TCMs followed a similar behaviour to sulphate and base metals through the year. The highest concentrations of TCMs were recorded 4 days after the onset of rainfalls due to the washout of evaporitic soluble salts, which resulted in a greater enrichment in dissolved TCMs than in major components (6-8 times) of evaporitic salts (i.e., Fe, S, Al, Ca and Mg). In the case of Tl, the peak did not coincide with these maximum values, but a few hours after the onset of rainfalls due probably to acid-induced release from jarosite or siliceous frustules of diatoms in the riverbed. After these washout processes, the concentration of most TCEs decreased progressively. However, Tl deviates from this tendency increasing its concentration in November and December due probably to the arrival of less evolved waters from the mining zone. After the intense rainfalls of March

and April, the lowest concentrations of TCMs were recorded due to dilution by runoff, being the river chemistry controlled by mixing of AMD from mine sites and freshwaters.

Flood events play an important role on the dissolved and particulate transport in AMD-affected rivers of semiarid regions. The remobilization of riverbed precipitates led to the transport of significant amounts of TCMs associated to particulate matter. However, element concentrations are not directly related to the concentration of particulate matter but to the nature of the minerals contained. The presence of REE, Sc, and Y, in the particulate matter seems to be associated to remobilized aluminosilicates or Al oxy-hydroxy-sulphates rather than Fe precipitates. However, in the case of Tl and Ga, the occurrence of these TCMs in the particulate matter appears to be associated with Fe minerals coating clay particles remobilized from the river bed during floods. Around 5.8 tonnes of REE, 1.3 tonnes of Y, 248 kg of Sc, 139 kg of Ga and 138 kg of Tl were delivered in its dissolved form by the Tinto River. Particulate loads of TCMs would add 10-30% to the dissolved one, depending on the TCM. These figures would imply that the Tinto River may transport into the oceans around 0.09% of the dissolved global flux of Y, 0.02% of REE, 0.01% of Ga and 0.001% of Sc.

Acknowledgements

This work was supported by the Spanish Ministry of Economy and Competitiveness through the research projects SCYRE (CGL2016-78783-C2-1-R), CAPOTE (CGL2017-86050-R) and VALOREY (RTI2018-101276-J-I00). The authors thank to Dr. Damiá Barceló (Co-Editor-in-Chief) and three anonymous reviewers for their helpful comments that notably improved the quality of the original manuscript.

References

Acero, P., Ayora, C., Torrento, C., Nieto, J.M., 2006. The behavior of trace elements during schwertmannite precipitation and subsequent transformation into goethite and

553 jarosite. Geochim. Cosmochim. Acta 70, 4130–4139.
554 https://doi.org/10.1016/j.gca.2006.06.1367.
555
556 Aguilar-Carrillo, J., Herrera-García, L., Reyes-Domínguez, I.A, Gutiérrez, E.J, 2020.
557 Thallium (I) sequestration by jarosite and birnessite: Structural incorporation vs surface
558 adsorption. Environ Poll 257, 113492. https://doi.org/10.1016/j.envpol.2019.113492.
559
560 Allison, J.D., Brown, D.S., Novo-Gradac, J., 1999. MINTEQA2/PRODEAFA2, a
561 geochemical assessment model for environmental systems: user manual supplement for
562 version 4.0. US EPA, NERL, Athens, Georgia.
563
564 Ayora, C., Macias, F., Torres, E., Lozano, A., Carrero, S., Nieto, J.M., Perez-Lopez, R.,
565 Fernandez-Martinez, A., Castillo-Michel, H., 2016. Recovery of rare earth elements and
566 yttrium from passive-remediation systems of acid mine drainage. Environ. Sci. Tech. 50,
567 8255–8262. doi:10.1021/ACS.EST.6B02084
568
569 Berger, A.C, Bethke, C.M, Krumhansl, J.L., 2006 A process model of natural attenuation
570 in drainage from a historic mining district. Appl. Geochem.15, 655-666.
571 https://doi.org/10.1016/S0883-2927(99)00074-8.
572
573 Buckby, T., Black, S., Coleman, M.L., Hodson, M.E., 2003. Fe-sulphate rich evaporative
574 mineral precipitates from the río Tinto, southwest Spain. Mineral. Mag. 67, 263–278.
575 https://doi.org/10.1180/0026461036720104.
576
577 Cánovas, C.R, Hubbard, C.G, Olías, M., Nieto, J.M, Black, S., Coleman, M.L, 2008.
578 Hydrochemical variations and contaminant load in the Río Tinto (Spain) during flood
579 events. J Hydrol 350, 24–40. https://doi.org/10.1016/j.jhydrol.2007.11.022.

580 Cánovas, C.R., Olías, M., Nieto, J.M., Galván, L., 2010. Wash-out processes of
581 evaporitic sulfate salts in the Tinto River: hydrogeochemical evolution and environmental
582 impact. Appl. Geochem. 25, 288–301.
583 https://doi.org/10.1016/j.apgeochem.2009.11.014.

584 Cánovas, C.R., Olías, M., Sarmiento, A.M., Nieto, J.M., Galván, L., 2012. Pollutant
585 transport processes in the Odiel River (SW Spain) during rain events. Water Resour.
586 Res. 48, W06508. https://doi.org/10.1029/2011WR011041.

587 Cánovas, C.R., Olías, M., Nieto, J.M., 2014. Metal(loid) attenuation processes in an
588 extremely acidic river: the rio Tinto (SW Spain). Water Air Soil Pollut. 225.
589 https://doi.org/10.1007/s11270-013-1795-7.

590 Cánovas, C.R, Macías, F, Olías, M, Basallote, MD, Pérez-López, R, Ayora, C, Nieto,
591 J.M., 2020. Release of technology critical metals during sulfide oxidation processes: the
592 case of the Poderosa sulfide mine (south-west Spain). Environ. Chem. 17, 93-104.
593 https://doi.org/10.1071/EN19118.

594 Carey, A.E, Nezat, C.A, Lyons, W.B, Kao, S.J, Hicks, D.M, Owen, J.S, 2002. Trace metal
595 fluxes to the ocean: the importance of high standing oceanic islands. Geophys Res Lett
596 29, 14-1–4. https://doi.org/10.1029/2002GL015690.

597 Casiot, C., Morin, G., Juillot, F., Bruneel, O., Personné, J.C., Leblanc, M., Duquesne, K.,
598 Bonnefoy, V., Elbaz-Poulichet, F., 2003. Bacterial immobilization and oxidation of
599 arsenic in acid mine drainage (Carnoulès creek, France). Water Res. 2003, 37, 2929-
600 2936. https://doi.org/10.1016/S0043-1354(03)00080-0.

601 Cobelo-García, A., Filella, M., Croot, P., Frazzoli, C., Du Laing, G., Ospina-Alvarez, N,
602 Rauch, S., Salaun, P., Schäfer, J., Zimmermann, S., 2015. COST action TD1407:
603 network on technology-critical elements (NOTICE) –from environmental processes to

human health threats. Environmental Science and Pollution Research International 22, 15188–15194. https://doi.org/10.1007/s11356-015-5221-0.

Deer, W.A., Howie, R.A., & Zussman, J., 2001. Framework Silicates: Feldspars, 2nd edn., Rock Forming Minerals, 4A; London, UK: The Geological Society, 972 pp.

Dutrizac, J.E., Chen, T.T, 2000. The behaviour of gallium during jarosite precipitation, Can. Metall. Q. 39 (1), 1–14. https://doi.org/10.1179/000844300794388949.

Dutrizac, J.E., Chen, T.T., Beauchemin, S., 2005. The behaviour of thallium(III) during jarosite precipitation. Hydrometallurgy 79, 138-153. https://doi.org/10.1016/j.hydromet.2005.06.003.

Gaillardet, J., Viers, J., Dupré, B., 2003. Trace elements in river waters. In: Turekian, K., Holland, H. (Eds.), Treatise on Geochemistry. Elsevier Science Publishers, New York, ISBN 0-08-044340-0, pp. 225–272.

Garbarino, J.R., Hoffman, G.L., 1999. Methods of Analysis by the U.S. Geological Survey National Water Quality Laboratory, Comparison of a nitric acid in-bottle digestion procedure to other whole-water digestion procedures, Open File Rep. 99-094, U.S. Geological Survey, Denver, Colorado.

Gómez-González, MA, García-Guinea, J., Laborda, F., Garrido, F., 2015b. Thallium occurrence and partitioning in soils and sediments affected by mining activities in Madrid province (Spain). Sci. Total Environ. 536, 268–278. http://dx.doi.org/10.1016/j.scitotenv.2015.07.033.

Gonzalez-Davila, M., Santana-Casiano, J.M., Laglera, L.M., 2000. Copper adsorption in diatom cultures. Mar. Chem. 70, 161–170. https://doi.org/10.1016/S0304-4203(00)00020-7.

Jamieson, H.E., Robinson, C., Alpers, C.N., McCleskey, R.B., Nordstrom, D.K., Peterson, R.C., 2005. Major and trace element composition of copiapite-group minerals

629 and coexisting water from the Richmond mine, Iron Mountain, California. Chem. Geol.
630 215, 387–405. https://doi.org/10.1016/j.chemgeo.2004.10.001.

631 Law, S., Turner, A., 2011. Thallium in the hydrosphere of south west England. Environ
632 Poll 159, 3484–3489. https://doi.org/10.1016/j.envpol.2011.08.029.

633 López-Arce, P., Garrido, F., García-Guinea, J., Voegelin, A., Göttlicher, J., Nieto, J.M.,
634 2019. Historical roasting of thallium- and arsenic-bearing pyrite: Current Tl pollution in
635 the Riotinto mine area. Sci Total Environ 648, 1263–1274.
636 https://doi.org/10.1016/j.scitotenv.2018.08.260.

637 Lozano, A., Ayora, C., Macías, F., León, R., Gimeno, M.J., Auqué, L., 2020.
638 Geochemical behavior of rare earth elements in acid drainages: Modeling achievements
639 and limitations. J Geochem Explor 216, 106577.
640 https://doi.org/10.1016/j.gexplo.2020.106577.

641 Mayes, W.M., Potter, H.A.B., Jarvis, A.P., 2010. Inventory of aquatic contaminant flux
642 arising from historical metal mining in England and Wales. Sci. Total Environ. 408, 3576-
643 3583. https://doi.org/10.1016/j.scitotenv.2010.04.021.

644 Meybeck, M., 2003. Global occurrence of major elements in rivers. In: Turekian, K.,
645 Holland, H. (Eds.), Treatise on Geochemistry. Elsevier Science Publishers, New York,
646 ISBN 0-08-044340-0, pp. 207–223.

647 Migaszewski, Z.M., Gałuszka, A., Migaszewski, A., 2014. The study of rare earth
648 elements in farmer's well waters of the Podwisniowka acid mine drainage area (south-
649 central Poland. Environ. Monit. Assess. 186, 1609-1622. https://doi.org/10.1007/s10661-
650 013-3478-7.

651 Nieto, J.M., Sarmiento, A.M., Cánovas, C.R., Olías, M., Ayora, C., 2013. Acid mine
652 drainage in the Iberian Pyrite Belt: 1. Hydrochemical characteristics and pollutant load of

653 the Tinto and Odiel rivers. Environ. Sci. Pollut. Res. 20, 7509–7519.
654 https://doi.org/10.1007/s11356-013-1634-9.

655 Noack, C. W.; Dzombak, D. A.; Karamalidis, A. K., 2014. Rare Earth Element
656 Distributions and Trends in Natural Waters with a Focus on Groundwater. Environ. Sci.
657 Technol. 48, 4317−4326.

658 Nordstrom, D.K., Wilde, F.D., 1998. Reduction–oxidation potential (electrode method).
659 In: National Field Manual for the Collection of Water Quality Data, Book 9, Chapter 6.5.
660 U.S. Geological Survey Techniques of Water-Resources Investigations, Reston, VA, pp.
661 1–22.

662 Nordstrom, D.K, 2011. Hydrogeochemical processes governing the origin, transport and
663 fate of major and trace elements from mine wastes and mineralized rock to surface
664 waters. Appl Geochem 26, 1777–1791.
665 https://doi.org/10.1016/j.apgeochem.2011.06.002.

666 Olías, M., Nieto, J.M, Sarmiento, A.M, Cerón, J.C, Cánovas, C.R, 2004. Seasonal water
667 quality variations in a river affected by acid mine drainage: the Odiel River (South West
668 Spain). Sci Total Environ 333, 267–81. https://doi.org/10.1016/j.scitotenv.2004.05.012.

669 Olías, M., Cánovas, C.R., Nieto, J.M., Sarmiento, A.M., 2006. Evaluation of the dissolved
670 load transported by the Tinto and Odiel rivers (South West Spain). Appl. Geochem. 21,
671 1733-1749. https://doi.org/10.1016/j.apgeochem.2006.05.009.

672 Olías, M., Nieto, J.M., 2015. Background conditions and mining pollution throughout
673 history in the Río Tinto (SW Spain). Environments 2, 295–316.
674 https://doi.org/10.3390/environments2030295.

675 Olías, M., Cánovas, C.R., Macías, F., Basallote, M.D., Nieto, J.M., 2020. The Evolution
676 of Pollutant Concentrations in a River Severely Affected by Acid Mine Drainage: Río
677 Tinto (SW Spain). Minerals 10, 598; doi:10.3390/min10070598.

678 Parkhurst, D.L., Appelo, C.A.J., 2013. Description of Input and Examples for PHREEQC
679 Version 3: A Computer Program for Speciation, Batch-Reaction, One-Dimensional
680 Transport, and Inverse Geochemical Calculations; US Geological Survey: Reston, VA,
681 USA, pp. 2328–7055.

682 Raymond, P.A, Oh N.H, 2009. Long term changes of chemical weathering products in
683 rivers heavily impacted from acid mine drainage: insights on the impact of coal mining in
684 regional and global carbon and sulphur budgets. Earth Planet Sci Lett 284, 50–6.
685 https://doi.org/10.1016/j.epsl.2009.04.006.

686 Resongles, E., Casiot, C., Freydier, R., Le Gall, M., Elbaz-Poulichet, F., 2015. Variation
687 of dissolved and particulate metal(loid) (As, Cd, Pb, Sb, Tl, Zn) concentrations under
688 varying discharge during a Mediterranean flood in a former mining watershed, the
689 Gardon River (France). J. Geochem. Explor. 158, 132–142.
690 http://dx.doi.org/10.1016/j.gexplo.2015.07.010.

691 Sánchez-España, J., Lopez Pamo, E., Santofimia, E., Aduvire, O., Reyes, J., Barettino,
692 D., 2005. Acid mine drainage in the Iberian Pyrite Belt (Odiel river watershed, Huelva,
693 SW Spain): geochemistry, mineralogy and environmental implications. Appl. Geochem.
694 20, 1320–1356. https://doi.org/10.1016/j.apgeochem.2005.01.011.

695 Sánchez-España, J., Yusta, I., Diez-Ercilla, M., 2011. Schwertmannite and
696 hydrobasaluminite: a re-evaluation of their solubility and control on the iron and
697 aluminium concentration in acidic pit lakes. Appl. Geochem. 26, 1752-1774.
698 https://doi.org/10.1016/j.apgeochem.2011.06.020.

699 Shiller, A.M, Frilot, D.M, 1996. The geochemistry of gallium relative to aluminum in
700 Californian streams. Geochim et Cosmochim Acta 60, 1323–1328.
701 https://doi.org/10.1016/0016-7037(96)00002-6.

702 Silva, Y.J.A.B., do Nascimento, C.W.A., da Silva, Y.J.A.B., Amorim, F. F., Cantalice,
703 J.R.B., Singh, V.P., Collins, A.L., 2018. Bed and suspended sediment-associated rare

earth element concentrations and fluxes in a polluted Brazilian river system. Environ Sci Poll Res, 25(34), 34426–34437. https://doi.org/10.1007/s11356-018-3357-4.

Tornos, F. (2006). Environment of formation and styles of volcanogenic massive sulfides: the Iberian Pyrite Belt. Ore Geology Reviews, 28(3), 259–307. https://doi.org/10.1016/j.oregeorev.2004.12.005.

Voegelin, A., Pfenninger, N., Petrikis, J., Majzlan, J., Plötze, M., Senn, A.C., Mangold, S., Steininger, R., Göttlicher, J., 2015. Thallium speciation and extractability in a thallium- and arsenic-rich soil developed from mineralized carbonate rock. Environ. Sci. Technol. 49, 5390-5398. https://doi.org/10.1021/acs.est.5b00629.

Webster, J.G., Swedlund, P.J., Webster, K.S., 1998. Trace metal adsorption onto an acid mine drainage iron(III) oxyhydroxysulfate. Environ. Sci. Technol., 32 (1998), pp. 1361-1368. https://doi.org/10.1021/es9704390.